Journal of Materials Science: Materials in Electronics
https://doi.org/10.1007/s10854-020-03701-3

Synthesis of nanocauliflower ZnO photocatalyst by potato waste and its photocatalytic efficiency against dye

Fahad A. Alharthi[1] · Nabil Al-Zaqri[1] · Adel El marghany[1] · Abdulaziz Ali Alghamdi[1] · Ali Q. Alorabi[2] · Neazar Baghdadi[3] · H. S. AL-Shehri[4] · Rizwan Wahab[5] · Naushad Ahmad[1]

Received: 8 March 2020 / Accepted: 27 May 2020

Abstract
Using different amount of potato peels, ZnO photocatalysts (ZO-PC) have been prepared by facile combustion process followed by the calcination at 500 °C for 10 min, and their obtained nanomaterials have been investigated through various techniques like powder X-ray diffraction (XRD), scanning electron microscope (SEM) combined with EDX, transmission electron microscope (TEM), Fourier transform infrared spectroscopy (FTIR), and UV–Vis spectroscopy in DRS mode. Moreover, the spectrophotometry technique has been employed to investigate the degradation of methylene blue (MB) under UV irradiation light ($\lambda < 400$ nm) by fabricated ZO-PCs. Among them, the lowest peel-containing sample was exhibited enhanced photocatalytic activity as compared to others also optical bandgap energy (E_g) was increased with increasing of peels from 3.39 to 3.49 eV.

1 Introduction

Sustainable modernization of society, industrial growth, and public unawareness of their rules and regulations are main causes of the generation of toxic pollutants in water ecosystem, which gives rise to motility and diseases in aquatic life, plants, human health, and alteration of weather and climates, relatively more effective in rural areas and undeveloped countries. At this very moment, it is considered as a plague for society due to release of toxic inorganic/organic waste byproducts or exhaust gases from industries into water reservoirs [1–5]. Dyes are the major pollutant, which contaminates various kinds of water bodies like seas, rivers, lakes, streams, waterways, and other geographical features where probability of chance for water navigations. In dyes industry: textile, dyeing, printing, paper, pulp, and paint are major resources of dyes that provide the characteristic color to the ingredients such as garments, paper, fabric, leather, and body paintings in ritual festivals [2, 3, 5, 6]. Many dyestuffs are toxic and carcinogenic in nature and affect the natural activities of both living and non-living creatures [5–8]. Therefore, it's a fundamental demand from the communities to protect them and accomplish of concern regulations; it must be important to degrade/depurate the dyes from polluted landscape and top priority to develop an advance and cost-effective method for their cure [7–10].

For the dye-contaminated system, researchers have established many degradation techniques such as adsorption, biodegradation, coagulation, electrochemical oxidation, flocculation, membrane separation, osmosis, and precipitation but each method has its own benefits and limitations [1, 5, 8, 11]. All of the above-mentioned approaches are not much effective, sensitive, and selective at trace level determination, time-consuming and inappropriate to degrade the chemically and structurally stable dyes. In last few decades, researchers have been focused to apply easier strategies to

Fahad A. Alharthi and Nabil Al-Zaqri have contributed equally to this work.

✉ Fahad A. Alharthi
fharthi@ksu.edu.sa

✉ Naushad Ahmad
anaushad@ksu.edu.sa

[1] Department of Chemistry, College of Science, King Saud University, Riyadh 11451, Kingdom of Saudi Arabia

[2] Department of Chemistry, Faculty of Science, Albaha University, Albaha 1988, Saudi Arabia

[3] Center of Nanotechnology, King Abdulaziz University, Jeddah, Saudi Arabia

[4] King Khalid Military Academy, Riyadh, Kingdom of Saudi Arabia

[5] Department of Zoology, College of Science, King Saud University, Riyadh 11451, Kingdom of Saudi Arabia

Published online: 01 June 2020

use natural and artificial light to decline and breakdown the dyestuff [12–14]. Among the different types of photolysis techniques, the photocatalysis with UV–Visible spectrophotometric methods are the most capable, simple, low-cost, eco-friendly process, and it has high efficiency for complete mineralization of photo-induced dyes such as methylene blue, methyl green, and rhodamine B dyes and other hazardous regents [6, 7, 15, 16]. In addition, obtained results are reproducible, more sensitive at low level quantitative and qualitative detection of colored and colorless reagents by applying the various certified methodologies [17, 18].

In past few years, metal-based nanomaterials (NMs) have been frequently used for the purification of dye-contaminated water through UV–Vis spectroscopy method [15–21]. To date, many research groups have to improved photocatalytic properties of metal oxides by the doping of noble metals, inorganic and organic semiconductors. For example, Meng et al. [22–28] synthesized numerous TiO_2 nanostructures (bandgap 3.2 eV) and its series of composites by the doping of non-toxic AgNPs, ZnO, CeO_2, Co_3O_4, and polymeric semiconductor like narrow bandgap (2.7 eV) graphite carbonitride (g-C_3N_4) by a cost-effective simple facile methods: solvothermal, hydrothermal, wet chemical reduction, sputtering, and deposition. And they demonstrated photocatalytic performances under the simulated sunlight/irradiation against the harmful dyes or chemicals, Rhodamine B (RhB), methyl orange (MO) or phenol with enhanced surface and photocatalytic properties as compared to commercial P25 because of improved reduced bandgaps, high surface area, coupling effects by charge separation, or electron–hole pairs. As compared to other metal oxide families, non-toxic biocompatible ZnO nanostructures have significant capacity to absorb photons/phonons in both regions, visible and near ultraviolet light due to high bandgap (3.37 eV), and it shows quantum confinement effect in UV–Visible region which is responsible for the degradation of organic dyes [2, 29–36]. Because of these properties, it can have used many advanced fields such as optical, dielectric, dye-sensitized solar cells, antibacterial agent, and medicinal with sensors applications.

For the fabrication of ZnO with different morphology, several synthetic approaches have been employed: physical, chemical, and thermal [29–43]. Recently, environmental-friendly green nanotechnology is economical branch of nanoscience for the design of the nanoscale products using either a fine powder or extract of plants/herbs as capping agents or stabilizers to control the crystal growth, and it provided manifold application in biological treatments, pharmaceutical, and water purification [44–47]. The principal aims of green synthesis are to develop high-performance nanomaterials by eliminating the use of toxic reagents and little/no hazard to our global system by potential exploring of herbs, plants, and their waste. The solution combustion method appears more favorable in terms of an economical high-yield, large-scale production and minimalism by using the plant waste materials and the avoidance of toxic chemicals and high energy ingredients for various types of nanostructures.

In this paper, zinc oxide photocatalysts (ZO-PCs) composed with nanocauliflowers were synthesized by low-cost homemade combustion technique using carbohydrate-rich potato wastes. The predominant form of this carbohydrate is starch, which is natural polymer, renewable and inexpensive, and acts as templates for NPs growth. The obtained materials were characterized with sophisticated instruments such as XRD, which is used to know the crystalline phase material whereas purity and morphology of the grown structures were examined SEM–EDX, TEM, and FTIR. The photocatalytic activity of fabricate samples with MB was measured by UV–Visible spectroscopy.

2 Materials and methods

2.1 Combustion synthesis of ZnO photocatalysts (ZO-PC)

Peel of potato as a fuel has been used for the fabrication of ZO-PCs by the combustion route. Fresh potatoes were purchased from a local market and its air-dried peels were grounded to fine powder and stored in an air-tight container. In brief, 2.97 g of zinc nitrate hexa hydrate ($Zn(NO_3)_2{\cdot}6H_2O$, 99.999%, Sigma-Aldrich, Germany) was dissolved in 10 mL of DI water and fine powder of waste in different mass fraction 0.297, 0.594, and 0.891 g were slowly added into it under stirring condition for 30 min. The mixture was transferred in borosil glass container and kept in a preheated muffle furnace at 500 °C for combustion process for 10 min. During this process, a large amount of heat and gases were evolved continuously; resulting white-colored voluminous porous nanopowder was obtained. For simplicity, prepared ZnO samples with different peel amount of 0.297, 0.594, and 0.891 g were termed as ZO-1PC, ZO-2PC, and ZO-3PC, respectively.

2.2 Characterization

The XRD patterns were employed for different samples using X-ray diffractometery (Rigaku Dmax-IIIA Japan) with $Cu_{K\alpha}$ radiation source ($\lambda = 1.5417$ Å) in 2θ range of 10–80°. The FTIR spectra were recorded at room temperature in the 4000–400 cm^{-1} range (Nicolet Avatar 360 FTIR) with KBr pellet method. The UV–Vis diffuse reflectance spectra (DRS) were measured in the range of 200–800 nm using a UV–Vis spectrophotometer (Jasco V-770, Japan). The morphology, particle size, and compositional analysis of photocatalysts were examined with SEM–EDX (Hitachi

S-4800, Japan) and TEM (JEOL JEM 1200EX, Japan). The chemical states and surface element compositions were determined by XPS in omicron with a monochromatic $Al_{K\alpha}$ radiation source and charge neutralizer. The C 1s line was taken as an internal standard at 284.6 eV. Both, wide-range survey spectra and detailed spectra for Zn 3p, O 1s,and C 1s were collected at 300 W.

2.3 Photocatalytic activity

Mineralization of MB by fabricated ZO-PCs was carried out on photocatalytic reactor; it has Hg-lamp ($\lambda_{max} = 365$ nm, 250 W) and quartz tube (L = 37 cm, ID = 2.3 cm) of 100 ml capacity. After the establishment of sorption (adsorption–desorption) equilibrium between 10 ppm aqueous solution of MB and 10 mg of synthesized catalyst, 2 ml centrifuged solution was taken out from reactor (30 min interval) and measured on spectrophotometer at 664 nm wavelength. A MB solution in absence of photocatalyst was used as control. The intensity of the main absorption peak (664 nm) of MB dye was referred to as a measure of the residual dye concentration. Following equation was used for the estimation of rate degradation:

$$\text{Degradation}(\%) = C_o - C_t/C_o \times 100 = A_o - A_t/A_o \times 100$$

where C_o is the initial concentration of dye solution, C_t is the dye concentration at certain reaction time t, A_o is the initial absorbance of dye solution, and A_t is the dye solution absorbance at a certain reaction time.

3 Results and discussion

3.1 X-ray diffraction

The XRD patterns of the prepared ZO-PCs are shown in Fig. 1. From all the diffraction peaks it's attributed to crystallinity of ZnO with the hexagonal wurtzite structure. The strong peaks are located at an angle (2θ) of 31.6°, 34.5°, and 36.2° corresponding to ⟨100⟩, ⟨002⟩ and ⟨101⟩, respectively, along with the other peaks are found at the angles 47.6° ⟨102⟩, 56.6° ⟨110⟩, 62.8° ⟨103⟩, 66.4° ⟨200⟩, 68.1° ⟨112⟩, 69.3° ⟨201⟩, 72.4° ⟨004 ⟩, and 77.0° ⟨202⟩ with their corresponding planes. The data obtained are in good agreement with JCPDF card no: 036-1451 for ZnO [48]. It is evident from the XRD plans that there are no extra peaks were observed which again indicates that the well-crystallinity and purity of as-synthesized ZnO nanostructures. It is noted that the major diffraction peaks' intensity and average crystallite size are decreased with amount of potato peels, and peaks' position is shifted slightly towards higher angle with increasing the potato peel contents. The average crystallite size can be calculated with the aid of Scherrer formula [49]. The calculated crystallite size values of ZO-PCs were found to be decreased from 21 to 10 nm.

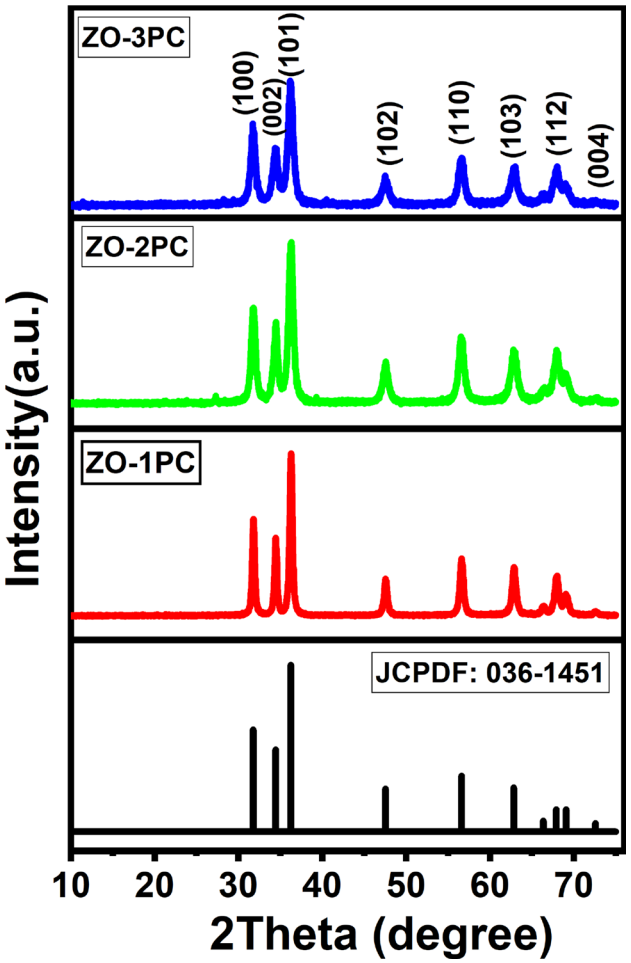

Fig. 1 X-ray diffraction pattern of ZO-PC nanopowders

3.2 Fourier transform infrared (FTIR) spectroscopy

Figure 2 shows the spectra of purity and functional characteristics of ZO-PCs in the range of 4000–400 cm^{-1}. Several well-defined peaks at 470, 850, 1259, 1380, and 3420 cm^{-1} have been observed in the spectra. The bands between 3600 and 3200 cm^{-1} corresponding to O–H mode of vibration, whereas a low intense bending vibration at 1627 cm^{-1} is the surface adsorbed water molecules [50, 51]. Strong absorption band between 440 and 470 cm^{-1} (ZO-1PC, ZO-2PC and ZO-3PC) was observed which is related with the metal oxide bond of ZnO [52]. The small peaks at 827–850 and 1380–1385 cm^{-1} are associated with the asymmetric and symmetric stretching bands of nitrate group (NO_3^{2-}), respectively [52]. In addition to observed peaks, no other peak related to any functional group was detected in the spectra,

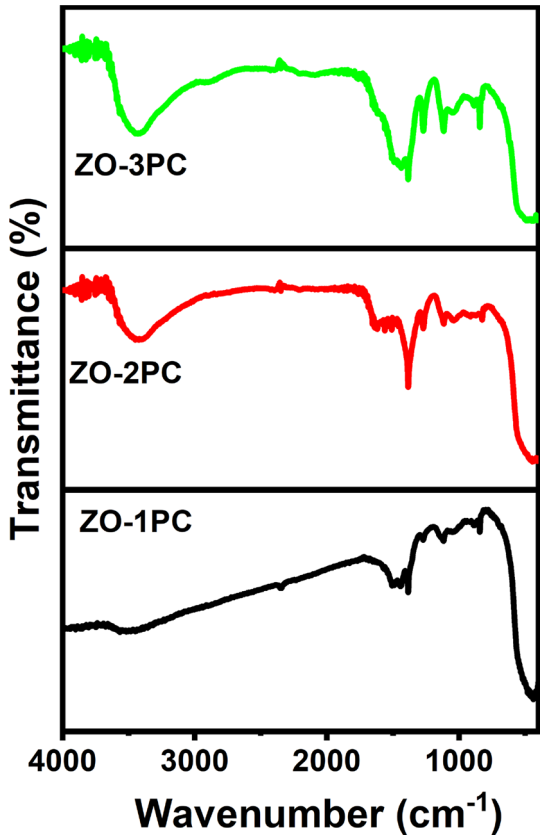

Fig. 2 FTIR spectra of ZO-PC nanopowders

which reveals that the synthesized nanostructures are pure ZnO without any significant impurities.

3.3 Morphological study

The morphology of the grown powder samples was analyzed via the scanning electron microscopy (SEM) and acquired data are presented as Fig. 3. Figure 3a shows the morphological detail of the sample ZO-1PC and it illustrates that several particles are presented in an array and form bunch similar to the cauliflower-like structures. The individual nanoparticle is very small in size (~ 10–15 nm) and is jointed with each other. Similar observation was also observed in another sample ZO-2PC, which seems that very small nanoparticles are scattered over the entire surface (Fig. 3b). The individual morphology of each nanoparticle is spherical, smooth, and very clear in shape. In another SEM image captured for the sample ZO-3PC, the NPs are joined with other particle through their bases in such a special manner that they made a beautiful cauliflower-shaped morphology and in an aggregated and clustered form. The full array of one flower-shaped structure is in the range of 3–4 µm (Fig. 3c). The quantitative/chemical compositions of three different ZO-PC cauliflower-shaped nanoparticles were also analyzed by EDX spectroscopy and are presented in Fig. 4a–f. All the spectra (Fig. 4b, d, f) indicate the presences of only Zn and O peaks without any impurity peaks.

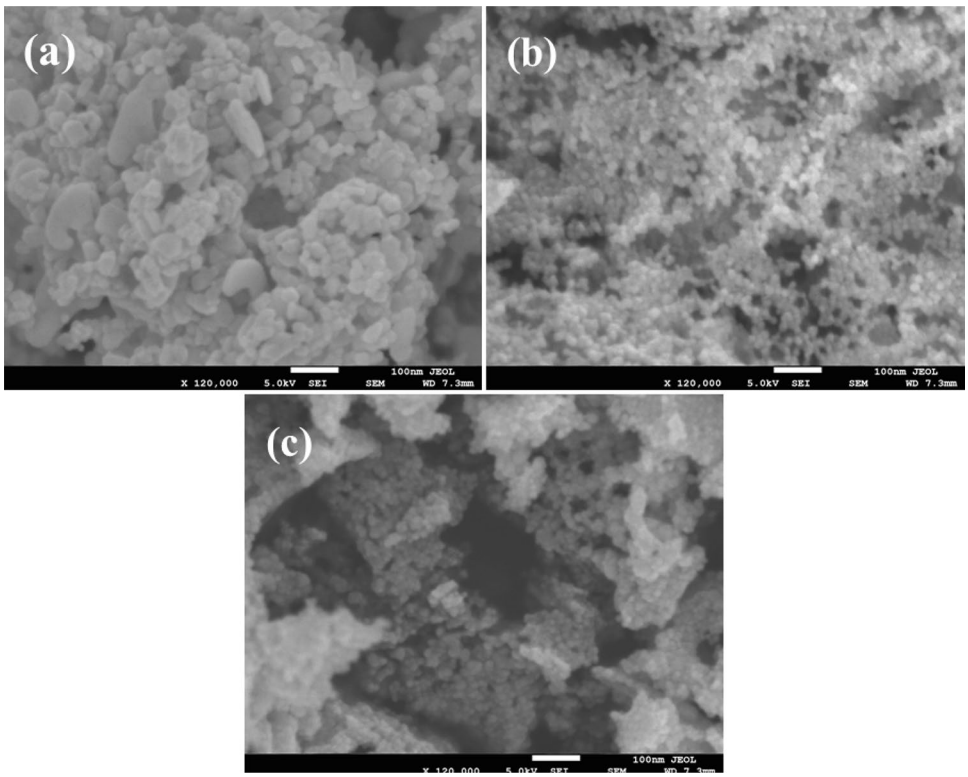

Fig. 3 SEM images of **a** ZO-1PC, **b** ZO-2PC, and **c** ZO-3PC

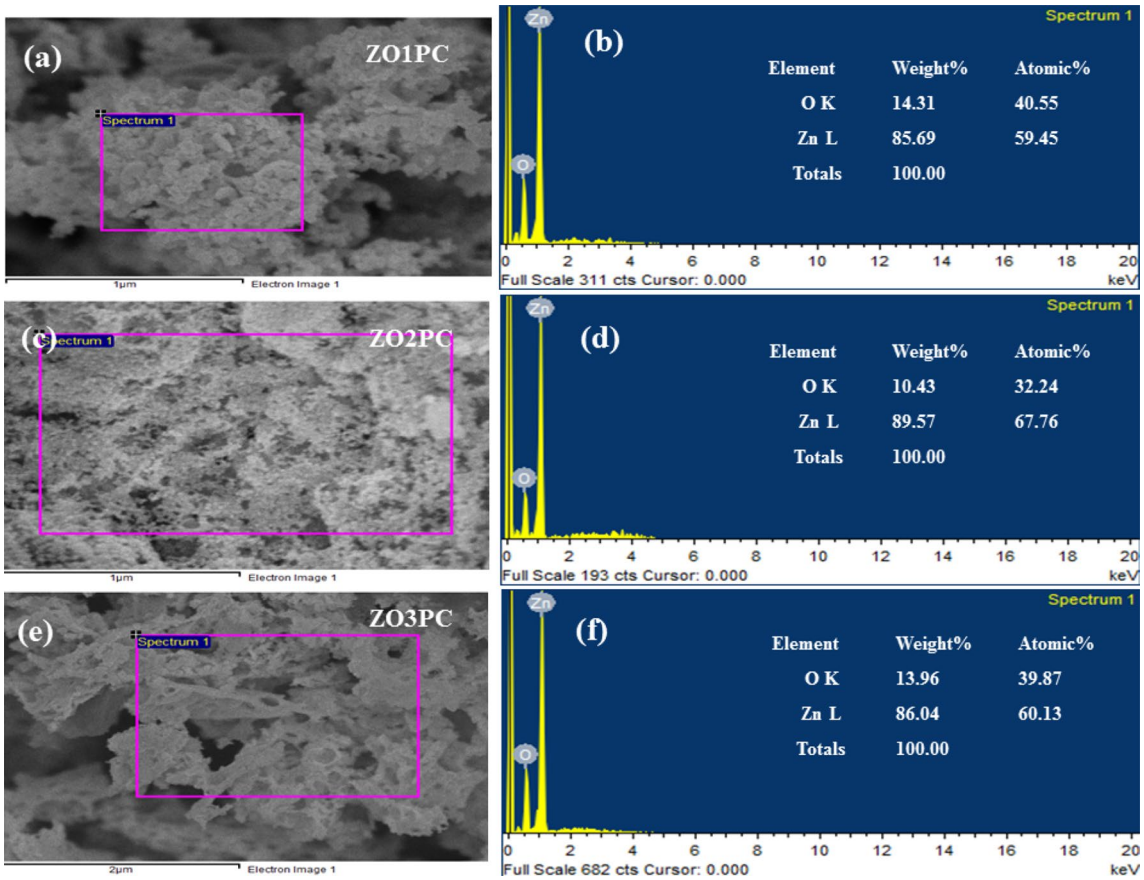

Fig. 4 EDX spectra with their corresponding elemental chemical compositions of ZO-PC

Further, the morphological examination was also accessed through transmission electron microscopy (TEM) at low & high magnification scales for the sample ZO-3PC and is presented in Fig. 5. The low magnified image (Fig. 5a) illustrates that the many nanoparticles are present, and these are detached with other structures. Further for more detailed observations, the size of an individual NP, the magnified image was selected and captured (Fig. 5b) and labeled (Fig. 5c) image of NPs. Fig. 5b, c elucidates that the average size of each NP ranges from 17 to 25 nm, with basis morphological characteristic such as spherical, smooth surfaces with high crystalline character. Here, it realizes that from the obtained results such as XRD and SEM, which are fully justified with the TEM images.

3.4 X-ray photoelectron spectroscopy (XPS) analysis

The elemental exploration for the selected sample ZO-3PC with full and core-level spectra of characteristic elements is depicted in Fig. 6. Initially, the wide scan survey was analyzed (Fig. 6a) and it shows the presence of Zn 2p, C 1s, and O 1s which represent that the prepared material is pure [53]. Narrow scan spectra (Zn 2p, C 1s, and O 1s) of ZO-3PC are shown in Fig. 6b–d. The peak for C 1s at binding energy of 285.6 eV was used as internal standard. It is established that the bands centered at 284.78 and 531.01 eV are associated with C 1s and O 1s, respectively [54]. The C 1s is centered at 284.38 eV for carbon, which might be due to atmospheric acquaintance to the sample (Fig. 6b), whereas O 1s peak is initiated at 531.01 eV with a shoulder at 532.42 eV (Fig. 6c). The two binding energy states at 1021.2 eV and 1044.3 eV are associated with the Zn $2p_{3/2}$ and Zn $2p_{1/2}$, respectively, which are very close to standard ZnO binding energy (Fig. 6d) [54].

3.5 UV–Vis diffuse reflectance spectra

The electronic structure of a semiconductor affects its optical property greatly, which reflects its photocatalytic property. Optical properties of prepared photocatalysts at room temperature were diagnosed in DRS mode. Figure 7a shows the UV-DRS spectra of prepared photocatalysts. The absorption edge is observed between 360 and 385 nm, which is shifted to smaller wavelength regions with higher peel contents. No other peak was observed in the spectrum confirms that the synthesized products are

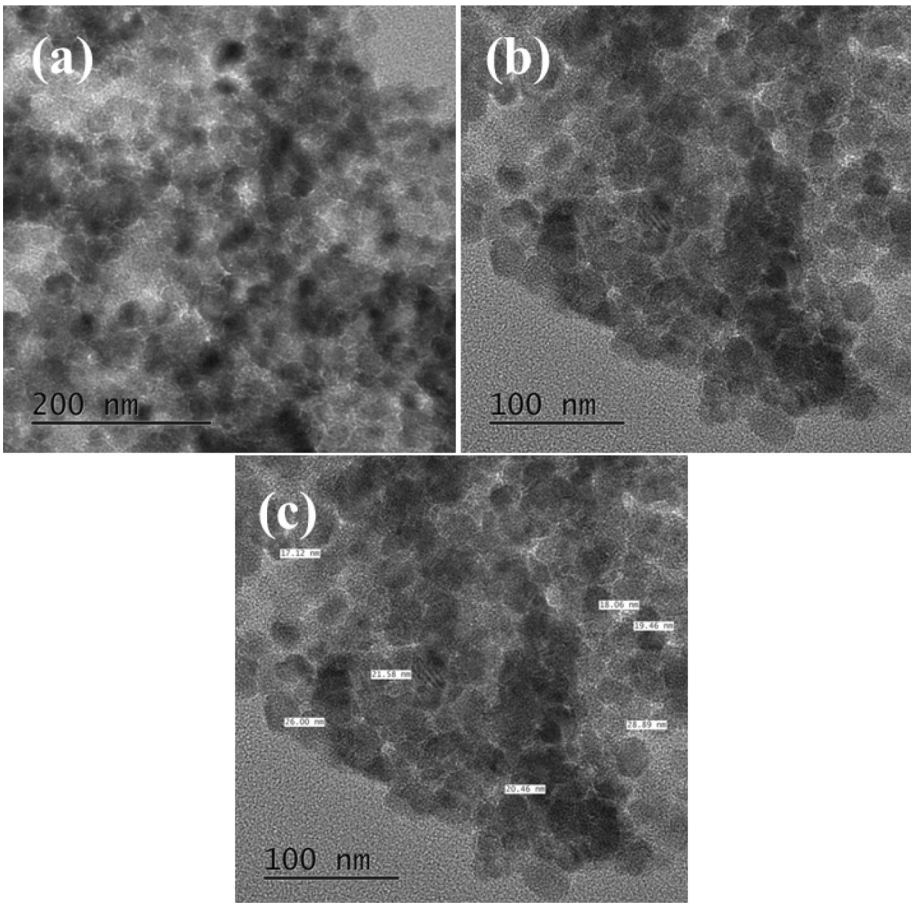

Fig. 5 Low (**a**) and high magnification (**b**, **c**) TEM images of ZO-3PC

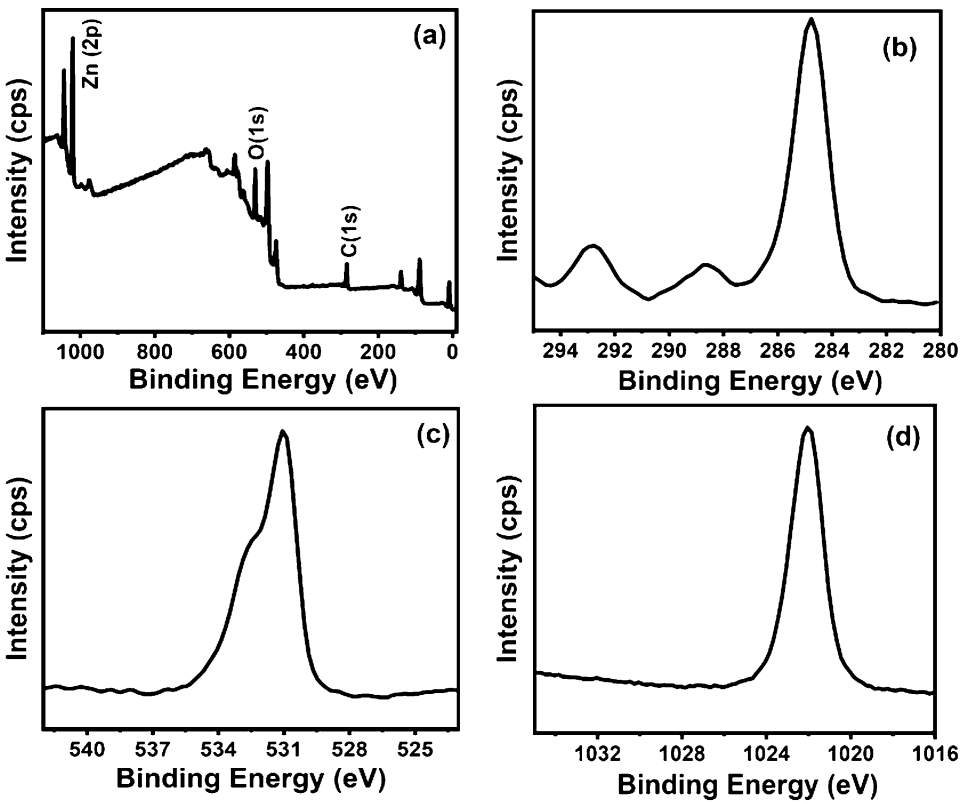

Fig. 6 XPS spectra of ZO-3PC: **a** survey **b** C 1s **c** O 1s and **d** Zn $2p_{3/4}$ spectra

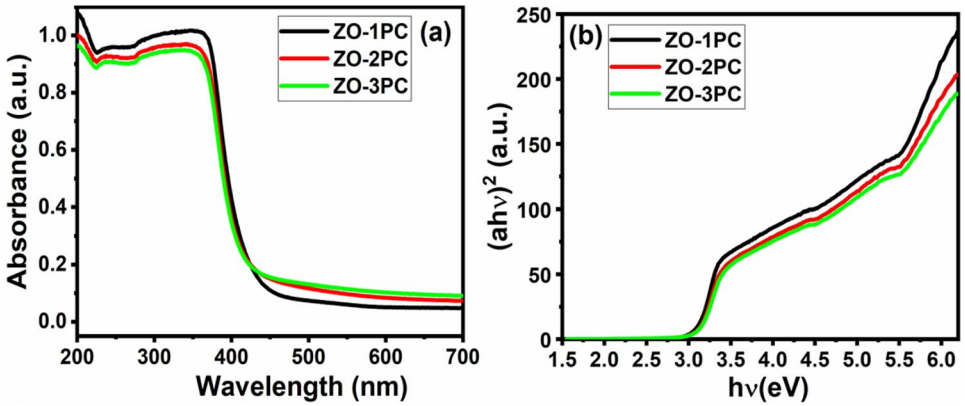

Fig. 7 UV–Vis absorption spectra of the ZO-PC **a** DRS spectra and **b** bandgap plots, where a.u denotes the arbitrary unit

ZnO only [55, 56]. The blue shift is attributed to quantum confinement effects due to reduced size of particles [57]. Estimation of bandgap energy is carried using Tauc plot that uses the value obtained from extrapolated linear slope to photon energy as shown in Fig. 7b. With increasing the peel content from 0.297 to 0.891 g, the bandgap energies of ZO-PCs are found to be increased from 3.39 to 3.49 eV, respectively, which can be assigned to the intrinsic bandgap absorption of ZnO due to the electron transitions from the valence band to the conduction band.

3.6 Photocatalytic activities in the degradation of MB

To represent the potential applications of as-synthesized ZnO products in waste water treatment, we have investigated the photocatalytic activities to decompose MB dye completely. Figure 8 shows the adsorption spectra and percentage degradative graph of MB solutions in presence of ZO-PCs (Fig. 8a–c) under UV light at different time intervals. The main absorption peak of MB centered at 664 nm before and after irradiation. When the light was turned on, the main peaks decreased continuously with increased irradiation time, indicating that MB solution was decomposed

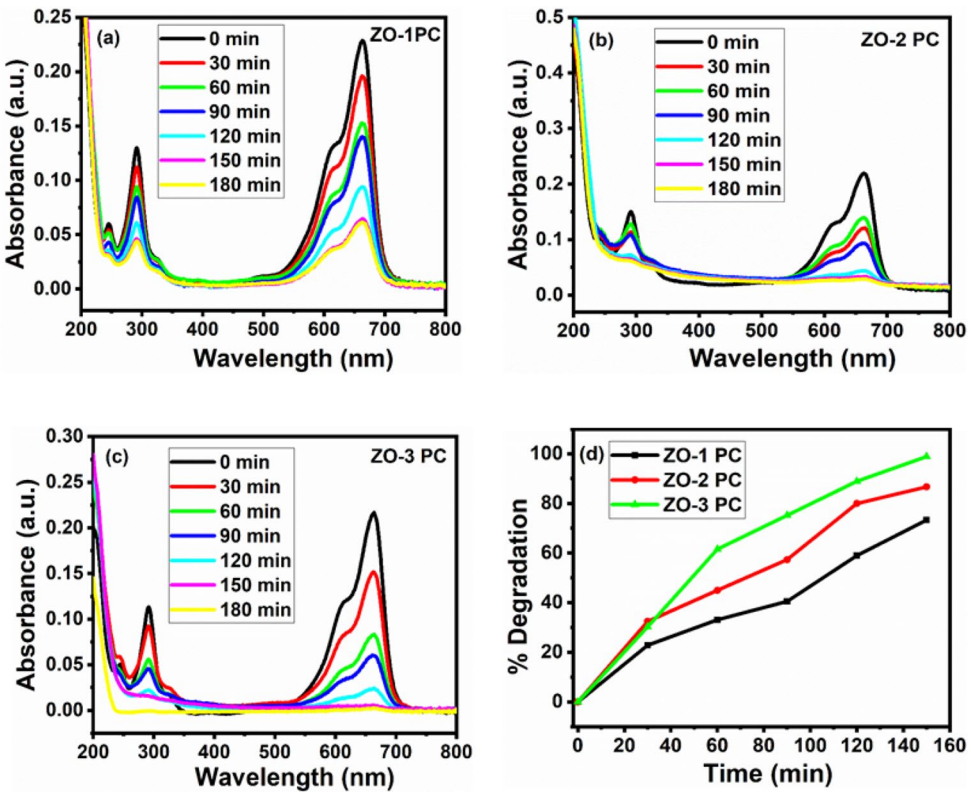

Fig. 8 Absorbtion spectra of different ZO-PC (**a**–**c**) in presence of MB and % degradation curves (**d**)

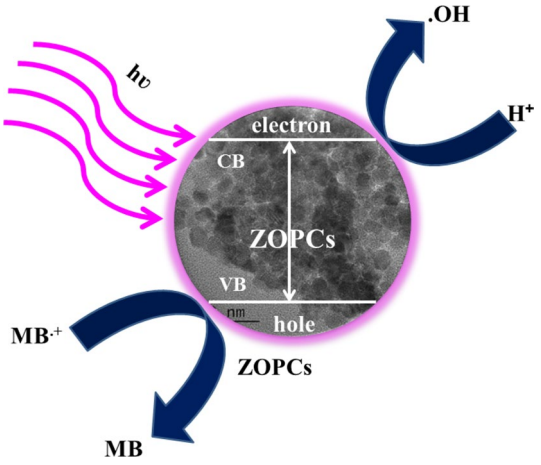

Fig. 9 Possible diagrammatic photodegradation process for ZO-PC with MB dye

in present system. When the illumination time is extended to 180 min, the color of MB solution completely disappeared. The absorption maxima corresponding to the aromatic hydrocarbon part were also decreased and it shows complete destruction of dye takes place in presence of the fabricated catalyst. The order of photocatalytic degradation rate of MB degradation rate was found to be ZO-PC1 (72%) < ZO-PC2 (87%) < and ZO-PC3 (99%), respectively (Fig. 8 d).

The decoloration of the used MB dye through the photocatalytic process with using three different types of zinc oxide nanoparticles similar to cauliflower-shaped structures were conducted for 180 min. As per the previous literature [3, 30, 32], once the degradation happens in an aqueous suspension, which is due to it forms electron and hole pair on the surface of the catalyst. The high oxidation of the hole (h_{VB}^{+}) in catalyst facilitates the direct oxidation of dye to reactive intermediates. The other reactive intermediate contributes to the available electron, which act as hydroxyl radical ($OH^{\cdot}$) in the photodegradation process. The hydroxyl group was generated by the decomposition of water molecule or through with reaction of hole and hydroxyl ion (OH^{-}) ions. As per the previous information [3, 30, 32], the hydroxyl radical is highly strong oxidant ($E^{0} = +3.06$ V) and responsible for the fractional to whole mineralization of numerous organic molecules. It's well known that the photocatalysis is a surface phenomenon, which depends on the active sites on the surfaces available for the reaction (as diagrammatic Fig. 9). In our case, the three types of zinc oxide nanoparticles (ZO-1PC, ZO-2PC, and ZO-3PC) have larger surface area and it presumes that the photocatalytic activity was anticipated and it's to be comparable with the commercial zinc oxide NPs. Due to larger surface properties of the prepared environmental-friendly NPs, it exhibits much greater photocatalytic efficiency as compared to other chemically grown NPs. Similar observations were also reports from the different authors [3, 30, 32], which shows their results on the basis of available large bandgap in the ZnO nanostructures. The large bandgap in ZnO deferments the electron–hole recombination process and because of this, it shows enhanced photocatalytic properties.

4 Conclusion

In conclusion, different nanoparticles which are ZnO nanocauliflowers were successfully synthesized through a simple and reliable combustion method using environmental-friendly and biocompatible potato waste products. The eco-friendly zinc oxide prepared via potato cover (peel) exhibits a crucial role for the structural architecture and catalytic enhancement. The as-synthesized ZnO nanostructures possess extraordinary catalytic activity to degrade the MB dye, which demonstrates the potential application towards the wastewater purification with environmental-friendly material. In this experiment, we received the enhanced catalytic efficiency for ZO-PCs which upsurge to 99.3% with 180 min UV light irradiation, which shows the prepared materials in excellent photocatalytic material for the larger industrial-scale exploitation.

Acknowledgements We thank the King Saud University, Deanship of Scientific Research, College of Science Research Centre for financial support.

References

1. L.W. Perelo, Review: in situ and bioremediation of organic pollutants in aquatic sediments. J. Hazard. Mater. **177**, 81–89 (2010)
2. H.H. Mohamed, Sonochemical synthesis of ZnO hollow microstructure/reduced graphene oxide for enhanced sunlight photocatalytic degradation of organic pollutants. J. Photochem. Photobiol. A **353**, 401–408 (2018)
3. S.K. Kansal, N. Kaur, Synthesis and characterization of titania nanoparticles for the photocatalytic degradation of 2-chlorophenol. Energy Environ. Focus **2**, 163–167 (2013)
4. J. Gong, F. Meng, Z. Fan, H. Li, Z. Du, Template-free controlled hydrothermal synthesis for monodisperse flowerlike porous CeO2 microspheres and their superior catalytic reduction of NO with NH3. J. Alloys Compd. **690**, 677–687 (2017)
5. A.V. Borhade, D.R. Tope, B.K. Uphade, An efficient photocatalytic degradation of methyl blue dye by using synthesised PbO nanoparticles. Eur. J. Chem. **9**, 705–715 (2012)
6. R.S. Rana, P. Singh, V. Kandari, R. Singh, R. Dobhal, S. Gupta, A review on characterization and bioremediation of pharmaceutical industries' wastewater: an Indian perspective. Appl. Water Sci. **7**, 1–12 (2017)
7. G.Z. Kyzas, J. Fu, K.A. Matis, The change from past to future for adsorbent materials in treatment of dyeing wastewaters. Materials **6**, 5131–5158 (2013)
8. G.Z. Kyzas, M. Kostoglou, Green adsorbents for wastewaters: a critical review. Materials **7**, 333–364 (2014)
9. J. Liu, H. Yu, L. Zhang, G. Zhang, J. Qu, H. Lv, Effect of greenhouse environment on organics migrating from agricultural

high-density polyethylene (HDPE) pipes. Sens. Lett. **11**, 1293–1297 (2013)
10. J. Wang, J. Liu, H. Xu, S. Ji, J. Wang, X. Tian, Hierarchical m-$BiVO_4$ microdendrites: hydrothermal template-free crystallization and their primary visible-light photocatalyst application. Energy Environ. Focus **2**, 79–84 (2013)
11. M.T. Yagub, T.K. Sen, S. Afroze, H.M. Ang, Dye and its removal from aqueous solution by adsorption: a review. Adv. Colloid Interfaces Sci. **209**, 172–184 (2014)
12. M.A. Quiroz, E.R. Bandala, C.A. Martinez-Huitle, Advanced oxidation processes (AOPs) for removal of pesticides from aqueous media, in *Pesticides—Formulations, Effects, Fate, Ch.34*, ed. by M. Stoytcheva (InTech, Mexico, 2011), pp. 685–705
13. V. Binas, D. Venieri, D. Kotzias, G. Kiriakidis, Modified TiO_2 based photo catalysts for improved air and health quality. J. Materiomics **3**, 3–16 (2017)
14. A.O. Ibhadon, P. Fitzpatrick, Heterogeneous photocatalysis: recent advances and applications. Catalysts **3**, 189–218 (2013)
15. A.K. Singh, U.T. Nakate, Photocatalytic properties of microwave-synthesized TiO_2 and ZnO nanoparticles using malachite green dye. J. Nanopart. **2013**, 7 (2013)
16. S. Panchal, R. Vyas, Use of undoped and iron doped zirconium dioxide in photocatalytic degradation of malachite green. Sci. Revs. Chem. Commun. **3**, 190–197 (2013)
17. E. Regulska, D.M. Brus, J. Karpinska, Photocatalytic decolourization of direct yellow 9 on titanium and zinc oxides. Int. J. Photoenergy (2013). https://doi.org/10.1155/2013/975356
18. S.Y. Pung, W.P. Lee, A. Aziz, Kinetic study of organic dye degradation using ZnO particles with different morphologies as a photocatalyst. Int. J. Inorg. Chem. (2012). https://doi.org/10.1155/2012/608183
19. S. Khan, M. Faisal, M.M. Rahman, A. Jamal, Exploration of CeO_2 nanoparticles as a chemi-sensor and photo-catalyst for environmental applications. Sci. Total Environ. **409**(2011), 2987–2992 (2011)
20. B. Karunagaran, P. Uthirakumar, S.J. Chung, S. Velumani, E.K. Suh, TiO_2 thin film gas sensor for monitoring ammonia. Mater. Charact. **58**, 680–684 (2007)
21. T.I. Edison, M.G. Sethuraman, Instant green synthesis of silver nanoparticles using *Terminalia chebula* fruit extract and evaluation of their catalytic activity on reduction of methylene blue. Process Biochem. **47**, 1351–1357 (2012)
22. Z. Fan, F. Meng, M. Zhang, Z. Wu, Z. Sun, A. Lia, Solvothermal synthesis of hierarchical TiO_2 nanostructures with tunable morphology and enhanced photo catalytic activity. Appl. Surf. Sci. **360**, 298–305 (2016)
23. R. Qin, F. Meng, M.W. Khan, B. Yu, H. Li, Z. Fan, J. Gong, Fabrication and enhanced photocatalytic property of TiO_2-ZnO composite photocatalysts. Mater. Lett. **240**, 84–87 (2019)
24. Z. Fan, F. Meng, J. Gong, H. Li, Y. Hu, Enhanced photocatalytic activity of hierarchical flower-like CeO_2/TiO_2 heterostructures. Mater. Lett. **175**, 36–39 (2016)
25. B. Yu, F. Meng, M.W. Khan, R. Qin, X. Liu, Facile synthesis of Ag NPs modified TiO_2@g-C_3N_4 heterojunction composites with enhanced photocatalytic activity under simulated sunlight. Mater. Res. Bull. **121**, 110641 (2020)
26. F. Meng, X. Song, Z. Sun, Photocatalytic activity of TiO_2 thin films deposited by RF magnetron sputtering. Vacuum **83**, 1147–1151 (2009)
27. F. Meng, Z. Sun, Enhanced photocatalytic activity of silver nanoparticles modified TiO2 thin films prepared by RF magnetron sputtering. Mater. Chem. Phys. **118**, 349–353 (2009)
28. B. Yu, F. Meng, M.W. Khan, R. Qina, X. Liu, Synthesis of hollow TiO_2@g-C_3N_4/Co_3O_4 core–shell microspheres for effective photooxidation degradation of tetracycline and MO. Ceram. Int. **46**, 13133–13143 (2020)
29. A.E. Suliman, Y. Tang, L. Xu, Preparation of ZnO nanoparticles and nanosheets and their application to dye-sensitized solar cells. Sol. Energy Mater. Sol. Cell **91**, 1658–1662 (2007)
30. R. Wahab, I.H. Hwang, Y.S. Kim, J. Musarrat, M.A. Siddiqui, H.K. Seo, S.K. Tripathy, H.S. Shin, Non-hydrolytic synthesis and photo-catalytic studies of ZnO nano particles. Chem. Eng. J. **175**, 450–457 (2011)
31. A. Yu, J. Qian, H. Pan, Y. Cui, M. Xu, L. Tu, Q. Chai, X. Zhou, Microlotus constructed by Fe-doped ZnO hierarchically porousnanosheets: preparation, characterization and gas sensing property. Sens. Actuators B **158**, 9–16 (2011)
32. R. Wahab, I.H. Hwang, Y.S. Kim, H.S. Shin, Photocatalytic activity of zinc oxide micro-flowers synthesized via solution method. Chem. Eng. J. **168**, 359 (2011)
33. R. Li, S. Yabe, M. Yamashita, S. Momose, S. Yoshida, S. Yin, T. Sato, Synthesis and UV-shielding properties of ZnO and CaO doped CeO_2 via soft solution chemical process. Solid State Ion. **151**, 235–241 (2002)
34. R. Salehi, M. Arami, N.M. Mahmoodi, H. Bahrami, S. Khorramfar, Novel bio compatible composite (Chitosan-ZnO nanoparticles): preparation, characterization and dye adsorption properties. Colloids Surf. B **80**, 86–93 (2010)
35. N. Mir, M. Salavati-Niasari, F. Davar, Preparation of ZnO nanoflowers and Zn glycerolate nanoplates using inorganic precursors via a convenient rout and application in dye sensitized solar cells. Chem. Eng. J. **181–182**, 779–789 (2012)
36. M. Salavati-Niasari, F. Davar, M. Mazaheri, Preparation of ZnO nanoparticles from [bis(acetylacetonato) zinc(II)]–oleylamine complex by thermal decomposition. Mater. Lett. **62**(12–13), 1890–1892 (2008)
37. D. Oh, W.J. Cho, T.W. Kim, Optical properties of ZnO nanoparticles embedded in a silicon nitride layer formed by sputtering and thermal treatment. Curr. Appl. Phys. **9**, e173–e175 (2009)
38. R.K. Jamal, M.A. Hameed, K.A. Adem, Optical properties of nanostructured ZnO prepared by a pulsed laser deposition technique. Mater. Lett. **132**, 31–33 (2014)
39. C. Zhao, Y. Huang, J.T. Abiade, Ferromagnetic ZnO nanoparticles prepared by pulsed laser deposition in liquid. Mater. Lett. **85**, 164–167 (2012)
40. K. Ogata, T. Komuro, K. Hama, K. Koike, S. Sasa, M. Inoue, M. Yano, Control of chemical bonding of the ZnO surface grown by molecular beam epitaxy. Appl. Surf. Sci. **237**, 348–351 (2004)
41. K. Li, H. Luo, T. Ying, One-step, solid-state reaction to ZnO nanoparticles in the presence of ionic liquid. Mater. Sci. Semicond. Process **14**, 184–187 (2011)
42. M.K. Debanath, S. Karmakar, Study of blueshift of optical band gap in zinc oxide (ZnO) nanoparticles prepared by low-temperature wet chemical method. Mater. Lett. **111**, 116–119 (2013)
43. W.M. Lee, Y.J. An, Effects of zinc oxide and titanium dioxide nanoparticles on green algae under visible, UVA, and UVB irradiations: no evidence of enhanced algal toxicity under UV preirradiation. Chemosphere **91**, 536–544 (2013)
44. S.M. Roopan, G. Elango, Exploitation of *Cocos nucifera* a non-food toward the biological and nanobiotechnology field. Ind. Crop. Prod. **67**, 130–136 (2015)
45. R. Atchudana, T.N.J.I. Edison, S. Perumal, Y.R. Lee, Green synthesis of nitrogen-doped graphitic carbon sheets with use of *Prunus persica* for supercapacitor applications. Appl. Surf. Sci. **393**, 276–286 (2017)
46. G. Zhang, X. Shen, Y. Yang, Facile synthesis of monodisperse porous ZnO spheres by a soluble starch-assisted method and their photocatalytic activity. J. Phys. Chem. C **115**, 7145–7152 (2011)
47. F. Renault, N. Morin-Crini, F. Gimbert, P.-M. Badot, G. Crini, Cationized starch-based material as a new ion exchanger adsorbent for the removal of CI acid blue 25 from aqueous solutions. Bioresour. Technol. **99**, 7573–7586 (2008)

48. A.K. Zak, W.H.A. Majid, M.R. Mahmoudian, M. Darroudi, R. Yousefi, Starch-stabilized synthesis of ZnO nanopowders at low temperature and optical properties study. Adv. Powder Technol. **24**, 618–624 (2013)
49. G. Srinivasan, R.R. Kumar, J. Kumar, Li doped and undoped ZnO nanocrystalline thin films: a comparative study of structural and optical properties. J. Sol–Gel Sci. Technol. **43**, 171–177 (2007)
50. A. Al-Hajry, A. Umar, Y.B. Hahn, D.H. Kim, Growth, properties and dye-sensitized solar cells–applications of ZnO nanorods grown by low-temperature solution process. Superlattices Microstruct. **45**, 529–534 (2009)
51. R.A. Nyquist, R.O. Kagel, *Infrared Spectra of Inorganic Compounds* (Academic Press Inc, London, 1971), p. 220
52. L. Wu, Y. Wu, L. Wei, Preparation of ZnO nanorods and optical characterizations. Physica E **28**(2005), 76–82 (2005)
53. V.H. Pham, T.V. Cuong, T.D. Nguyen-Phan, H.D. Pham, E.J. Kim, S.H. Hur, E.W. Shin, S. Kim, J.S. Chung, One-step synthesis of superior dispersion of chemically converted graphene in organic solvents. Chem. Commun. **46**(24), 4375–4377 (2010)
54. B. Vincent Crist, *Handbook of Monochromatic XPS Spectra: The Elements and Native Oxides* (Wiley, Chichester, 2000), p. 510
55. Y.H. Ni, X.W. Wei, J.M. Hong, Y. Ye, Hydrothermal preparation and optical properties of ZnO nanorods. Mater. Sci. Eng. B **121**, 42–47 (2005)
56. S.C. Lyu, Y. Zhang, H. Ruh, H.J. Lee, H.W. Shim, E.K. Suh, C.J. Lee, Low temperature growth and photoluminescence of well-aligned zinc oxide nanowires. Chem. Phys. Lett. **363**, 134–138 (2002)
57. X. Zhao, M. Li, X. Lou, Sol–gel assisted hydrothermal synthesis of ZnO microstructures: morphology control and photocatalytic activity. Adv. Powder Technol. **25**, 372–378 (2014)